ARTICLES
PUBLISHED ONLINE: 15 JULY 2012 | DOI: 10.1038/NPHOTON.2012.158
nature photonics

Broadband dye-sensitized upconversion of near-infrared light

Wenqiang Zou[1], Cindy Visser[1], Jeremio A. Maduro[1], Maxim S. Pshenichnikov[2] and Jan C. Hummelen[1,2]*

Photon upconversion of near-infrared photons is a promising way to overcome the Shockley–Queisser efficiency limit of 32% of a single-junction solar cell. However, the practical applicability of the most efficient known upconversion materials at moderate light intensities is limited by their extremely weak and narrowband near-infrared absorption. Here, we introduce the concept of an upconversion material where an organic near-infrared dye is used as an antenna for the β-$NaYF_4$:Yb,Er nanoparticles in which the upconversion occurs. The overall upconversion by the dye-sensitized nanoparticles is dramatically enhanced (by a factor of ∼3,300) as a result of increased absorptivity and overall broadening of the absorption spectrum of the upconverter. The proposed concept can be extended to cover any part of the solar spectrum by using a set of dye molecules with overlapping absorption spectra acting as an extremely broadband antenna system, connected to suitable upconverters.

One of the fundamental factors limiting the energy conversion efficiency of a single-junction solar cell to the Shockley–Queisser limit of ∼32% is the inability to absorb photons with energy less than the bandgap of the active materials[1]. Upconversion materials, which can sum the energies of near-infrared (NIR) quanta to emit a quantum of higher energy, are considered to be one of the promising routes to overcoming this limit[2–6]. Other methods focus on adapting the absorption of the solar cell active-layer materials to the solar spectrum, but upconversion modifies the solar spectrum to make it match better with the absorption spectrum of the solar cells. This strategy also makes it possible to electrically isolate the upconverters from the active layer and apply them as a separate layer in solar cells.

In theory, the standard AM1.5 spectrum power conversion efficiency of a single-bandgap solar cell can be increased by up to 50.7% by the application of an ideal upconverter (with the two upconverter bandgaps at 0.94 and 1.40 eV), in combination with a photovoltaic active-layer material with a relatively wide bandgap of 2 eV (ref. 7). However, to date, the upconversion solar cell efficiencies obtained experimentally have been extremely low and merely serve as proof of principle[3,8–12]. The main problem is that the known internally efficient upconversion materials absorb extremely weakly and within a very narrow spectral window. Moreover, upconversion is a process that is of higher order in light intensity (that is, quadratic in intensity for two-photon upconversion in the low-intensity limit), making very high illumination intensities often necessary. The best upconversion materials are currently based on mixed lanthanide compounds[11,13]. Promising upconversion efficiencies have also been reported using (supra)molecular triplet–triplet annihilation systems[14–16], but the spectral range of 650–700 nm to be upconverted is of limited relevance for solar cell applications. Of these materials, bulk $NaYF_4:Er^{3+},Yb^{3+}$ and $NaYF_4:Er^{3+}$ have shown the highest upconversion quantum yields under monochromatic irradiation at 975 nm and 1,522 nm NIR light (5% and 3%, respectively[11,17]). The corresponding $NaYF_4:Er^{3+}$(2%),Yb^{3+}(20%) nanoparticles typically show lower, size-dependent quantum yields; for example, 0.1% has been reported for 30-nm-diameter particles[17]. The inherently weak and narrowband absorption of Ln^{3+} ions in such materials is due to the parity-forbidden nature of the 4*f* transitions. Hence, most of the efforts to enhance Ln^{3+} upconversion luminescence have focused on materials providing a locally enhanced electromagnetic field or on doping with other lanthanide ions, serving as sensitizers[18–20]. For instance, plasmonic coupling was introduced to enhance the upconversion efficiency of lanthanide nanoparticles[21–27], resulting in enhancement factors of 2 to 8 (refs 21–23). More recently, the upconversion luminescence of gold-decorated β-$NaYF_4$:Yb,Tm nanoparticles at 345 nm was reported to be increased by a factor of 109 (ref. 27).

Here, we propose and demonstrate the viability of a new strategy to enhance the upconversion luminescence of lanthanide nanoparticles based on increased and spectrally broadened absorption, using organic infrared dyes as sensitizers. The main idea was inspired by the natural light-harvesting systems in which various absorber molecules surround and transfer the solar energy to the central reaction centre[28], albeit for upconversion instead of charge transfer. In our approach, dye molecules function as antennas, absorbing incident light and transferring their excitation energy to the upconverting metal ions encapsulated in a nanoparticle (Fig. 1). In a solar cell, the upconverted photon energy is then transferred radiatively or non-radiatively to the active layer. The advantages of combining organic antennas with inorganic upconversion centres are (i) the strong NIR absorption, (ii) the broad absorption spectrum, (iii) the ability to tune the absorption band by molecular bandgap engineering, and (iv) the possibility of using a set of complementary antenna molecules to further optimize the absorption range (for example, in an energy cascade manner).

We chose to show the first proof of principle of dye sensitization using nanoparticle upconverters for 975 nm light, for chemical and instrumental reasons. Oleylamine-coated β-$NaYF_4$:Yb,Er nanoparticles with an average core diameter of 16 nm were prepared using a known method from a mixture of trifluoroacetates in oleylamine[29]. Solutions of these nanoparticles in $CHCl_3$ showed the characteristic bright green-yellow upconversion emission following excitation

[1]Stratingh Institute for Chemistry, University of Groningen, Nijenborgh 4, 9747 AG Groningen, The Netherlands, [2]Zernike Institute for Advanced Materials, University of Groningen, Nijenborgh 4, 9747 AG Groningen, The Netherlands. *e-mail: j.c.hummelen@rug.nl

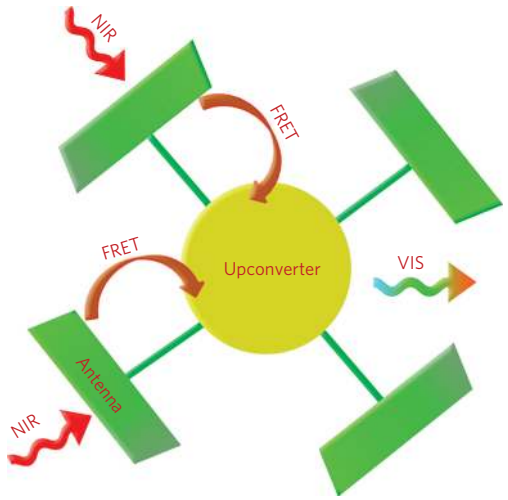

Figure 1 | Principal concept of the dye-sensitized nanoparticle. Antenna dyes (green) absorb NIR solar energy (red wavy arrows) and transfer it (brown arrows) to the nanoparticle core (in yellow), where upconversion occurs. Upconversion denotes a nonlinear (on the incident radiation intensity) process in which the energies of two NIR quanta are summed to emit a quantum of higher energy in the green-yellow region (green-yellow wavy arrow).

with ~975 nm laser light. A commercially available cyanine dye, IR-780, was selected as the starting material for the preparation of functionalized antenna molecules to be attached to the surface of the nanoparticles. Nucleophilic substitution of the central chlorine atom in IR-780 was used as the method to prepare a carboxylic acid-functionalized derivative (see Supplementary Sections A–C for details). The resulting carboxylated dye absorbs light mainly between 650 and 850 nm, with a maximum at 806 nm in $CHCl_3$ (Fig. 2a); we therefore named it IR-806. The extinction coefficient of IR-806 at 806 nm is 390 l g^{-1} cm^{-1}, which is ~5 × 10^6 times higher than that of β-$NaYF_4$:Yb,Er nanoparticles at 975 nm (7 × 10^{-5} l g^{-1} cm^{-1}). Weak absorption of IR-806 below 600 nm is also essential, because the antenna dye should be transparent for the upconverted photons that exit the nanoparticle.

At 750 nm excitation, the emission spectrum of IR-806 in $CHCl_3$ extends well beyond 900 nm (Fig. 2b). The overlap between the emission spectrum of IR-806 and the absorption spectrum of the nanoparticles at 900–1,000 nm, albeit not optimal, still allows for Förster-type energy transfer from excited IR-806 to the Yb^{3+} absorption centres in the nanoparticles. The exchange reaction with the oleylamine ligands and binding of IR-806 to the surface of the nanoparticle were determined by clearly observable changes of absorption in the NIR and infrared regions as well as in the emission properties (Supplementary Figs S6–S8). First, following the addition of oleylamine-coated nanoparticles to a solution of IR-806 in $CHCl_3$, the absorption of IR-806 at 806 nm decreased and the absorption maximum wavelength gradually blueshifted from 806 nm to a saturation value of 800 nm (Supplementary Fig. S7a). Second, the IR-806 luminescence decreased to 35% of the original intensity (Supplementary Fig. S8a). In a blank experiment in which IR-806 was bound to oleylamine-coated $NaYF_4$ nanoparticles with no Yb and Er photon energy acceptors, an identical blueshift in IR-806 absorption was observed (Supplementary Fig. S7b), but the luminescence decrease was only to 90% of the original intensity (Supplementary Fig. S8b). Third, the lifetime of IR-806 luminescence shortened from 1.14 ns (pure IR-806) to 0.64 ns (IR-806:nanoparticle) upon binding to the $NaYF_4$:Yb,Er nanoparticles (Supplementary Fig. S9). This set of experiments

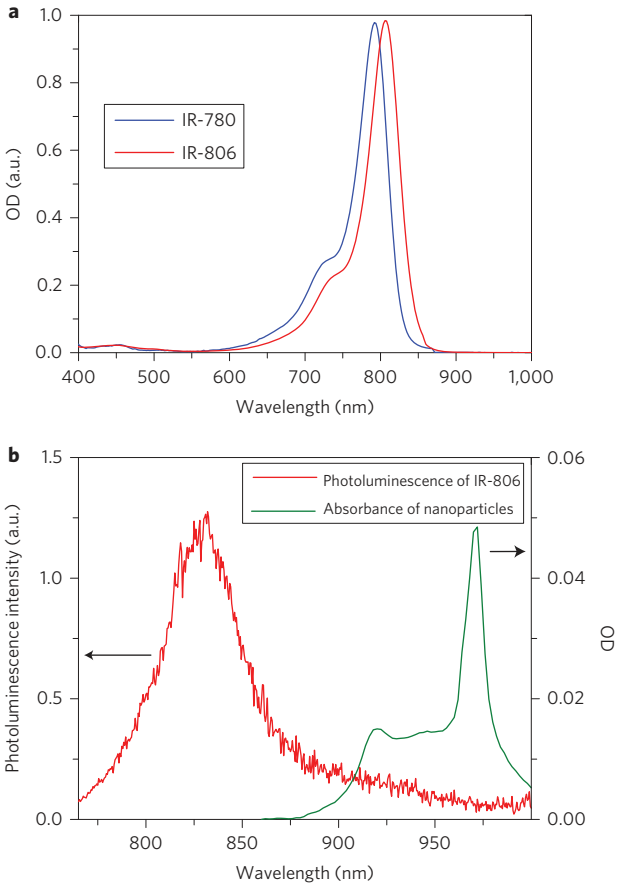

Figure 2 | Absorption and emission spectra. a, Absorption spectra of IR-780 (3.0 × 10^{-6} M; blue line) and carboxylic acid derivative IR-806 (3.18 × 10^{-6} M; red line) in $CHCl_3$. **b**, Emission spectrum of IR-806 in $CHCl_3$ (3.18 × 10^{-6} M; red line) and absorption spectrum of oleylamine-coated β-$NaYF_4$:Yb,Er in $CHCl_3$ (green line). OD, optical density.

demonstrates that ~50% of the photon energy initially absorbed by bound IR-806 is transferred to the Yb and Er energy-accepting ions in the $NaYF_4$:Yb,Er nanoparticle core.

This conclusion was also verified by similar measurements on the original IR-780 (which cannot bind to the nanoparticles) instead of IR-806; no changes in IR-780 absorption and emission were observed (Supplementary Figs S10,S11). Finally, the Fourier transform infrared (FTIR) spectrum of a sample of dried and washed dye-coated nanoparticles resembles a superposition of the two spectra of oleylamine-coated nanoparticles and the dye (Supplementary Fig. S6). This strongly suggests that close proximity of the dye (secured by chemisorption in the case of IR-806) and nanoparticle is necessary for efficient energy transfer.

The upconversion spectrum of the solution containing IR-806-functionalized nanoparticles under 800 nm, 2 mW continuous-wave (c.w.) laser excitation is shown in Fig. 3a. There are three characteristic Er^{3+} emission bands at 510–530 nm, 530–570 nm and 630–680 nm, corresponding to $^2H_{11/2} \rightarrow {}^4I_{15/2}$, $^4S_{3/2} \rightarrow {}^4I_{15/2}$ and $^4F_{9/2} \rightarrow {}^4I_{15/2}$ transitions, respectively[27]. The 500–700 nm spectral distribution of upconverted light from the IR-806/nanoparticles samples irradiated at 800 nm (2 mW) was determined to be similar to that of samples of pure nanoparticles irradiated at 975 nm (50 mW) (Supplementary Fig. S12). This clearly indicates that the 800 nm photon energy is absorbed by IR-806, transferred to the nanoparticle core, upconverted to a higher photon energy, and subsequently re-emitted. In the cases of solutions of pure oleylamine-capped nanoparticles, pure IR-806 in $CHCl_3$ (800 nm

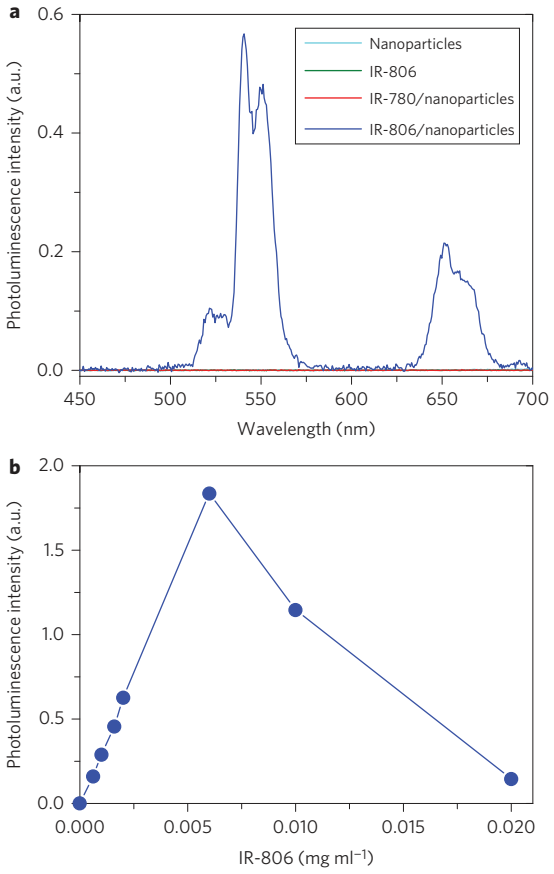

Figure 3 | Upconversion emission intensities. a, Steady-state emission spectra of β-$NaYF_4$:Yb,Er nanoparticles (cyan line, no spectrum produced), IR-806 (green line, no spectrum produced), β-$NaYF_4$:Yb,Er nanoparticles/IR-780 (0.80/0.006 mg ml^{-1}; red line) and β-$NaYF_4$:Yb,Er nanoparticles/IR-806 (0.80/0.006 mg ml^{-1}; blue line) in $CHCl_3$ excited by a 2 mW, 800 nm c.w. laser. **b**, Emission intensity integrated in the range 500–685 nm of β-$NaYF_4$:Yb,Er nanoparticles (0.80 mg ml^{-1}) as a function of IR-806 content (in $CHCl_3$) excited by a 2 mW, 800 nm c.w. laser.

excitation) and mixtures of non-functionalized IR-780 and nanoparticles (780 nm excitation), no detectable upconversion emission was observed, in full agreement with the absorption and fluorescent quenching experiments. Therefore, we conclude that functionalized IR-806 (secured by chemisorption) acts as an antenna for the β-$NaYF_4$:Yb,Er nanoparticles for the upconversion process.

We next determined the optimal surface coverage of the nanoparticles by antenna molecules so as to achieve the most efficient dye-sensitized upconversion (Fig. 3b). On adding IR-806 to a solution of nanoparticles, the upconversion emission intensity first increases, which is consistent with an increasing overall absorption of the excitation energy at 800 nm by an increasing number of surface-bound antenna molecules. However, beyond a certain concentration, the further increase in the IR-806/nanoparticle ratio results in a decreasing upconversion emission intensity. The observed decline can be explained by two factors: increased mutual interactions between antenna molecules on the nanoparticle surface (self-quenching) and an increasing concentration of unbound (excess) antenna molecules, which absorb the excitation energy but do not transfer it to the nanoparticles. The optimum IR-806:nanoparticle weight ratio was determined as 1:133. We estimate that a mean of 70 ± 20 antenna molecules per average sized nanoparticle are bound at this ratio, with a centre-to-centre intermolecular distance of ~3.4 nm (Supplementary Section E). This optimal concentration was used in all subsequent experiments.

Figure 4 shows the upconversion emission intensity integrated in the range 500–685 nm as a function of incident power. The best fit with a power function results in a perfect quadratic dependence on the incident light intensity. This confirms that the mechanism of the antenna-mediated process involves a two-photon upconversion step. Based on this set of observations we propose the following mechanism for the overall process in the IR-806/nanoparticles solution, and call it 'dye-sensitized upconversion' (DUC). In this mechanism, the bound IR-806 antenna molecules absorb the NIR photons and transfer their excitation energy to the Yb^{3+} $^2F_{5/2}$ level by resonance energy transfer. The typical energy transfer processes from Yb^{3+} to Er^{3+} follow[13], eventually leading to the Er^{3+} emission of upconverted light.

The monochromatic quantum yield (mQY) of the IR-806/nanoparticles was determined at an excitation wavelength of 800 nm as $0.12^{+0.10}_{-0.05}$% at the intensity saturation point (Fig. 4) for monochromatic illumination (for details see Supplementary Section F). The mQY of our non-sensitized oleylamine-coated nanoparticles was measured to be 0.3 ± 0.1% at the maximum absorption wavelength of 975 nm. This value is in good agreement with the reported mQY value[17] of 0.1% for slightly larger (30 nm diameter) but otherwise similar oleylamine-coated nanoparticles given the higher intensities used here. The two mQYs are, within experimental error, in reasonable agreement with the observed luminescence quenching and excited-state lifetime shortening of the nanoparticle-bound dye described above.

The upconversion action spectrum (that is, upconverted power as a function of excitation wavelength) was recorded using a 2 mW calibrated wavelength-tunable c.w. laser. It was first confirmed that the emission spectrum of the sample was independent of the excitation wavelength in the 720–1,000 nm spectral range. The integrated power over the 500–685 nm range of the emission was then plotted versus excitation wavelength (Fig. 5). The upconversion action peak in the range 740–850 nm corresponds to the squared absorption of IR-806, and the tiny action peak in the 900–990 nm range follows the squared absorption of β-$NaYF_4$:Yb,Er (Fig. 5, inset). This is fully consistent with the proposed DUC mechanism comprising a two-photon process in which the antenna molecules are involved as initial absorbers.

The dramatic effect of the dye-sensitized process is immediately evident from the main panel, where the contribution from

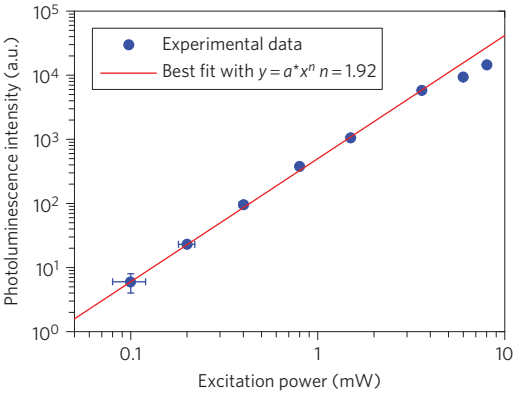

Figure 4 | Upconversion photoluminescence intensity as a function of excitation power. Integrated in the range 500–685 nm, upconversion intensity of β-$NaYF_4$:Yb,Er nanoparticles/IR-806 (0.80/0.006 mg ml^{-1}) in $CHCl_3$ as a function of excitation power from an 800 nm c.w. laser. A best fit with a power function yields the exponent factor $n = 1.92$, indicating a purely two-photon process.

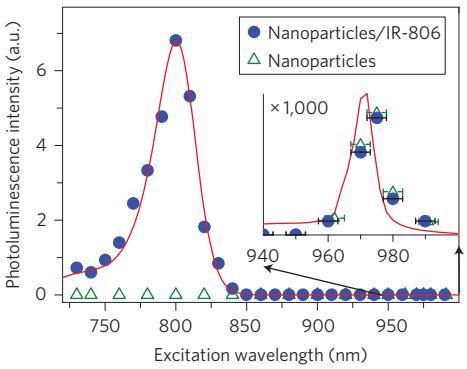

Figure 5 | Upconversion action spectra. Experimental upconversion excitation spectra of β-$NaYF_4$:Yb,Er nanoparticles/IR-806 (0.80/0.006 mg ml^{-1}; blue circles) and β-$NaYF_4$:Yb,Er nanoparticles (0.80 mg ml^{-1}; green triangles), both dissolved in $CHCl_3$. The emission intensity is integrated in the 500–685 nm range with excitation from a 2 mW c.w. laser. The red line shows the squared absorption spectrum. Inset: wavelength range from 940 to 1,000 nm, magnified by a factor of 1,000.

upconversion by the non-sensitized process around 975 nm is simply invisible on this scale. However, as the inset shows, the non-sensitized upconversion does take place in this range. Importantly, this process has a similar efficiency and spectral response for non-coated and dye-coated nanoparticles, which proves that the upconversion properties of the nanoparticles were not compromised following dye attachment. Although the peak-to-peak (at 975 nm versus at 800 nm) ratio of non-sensitized and sensitized upconversion is ~1:1,100, the integrated spectral response in the 720–1,000 nm range from the dye-coated nanoparticles, as shown in Fig. 5, is ~3,300 times stronger than that of the non-sensitized nanoparticles. This result lends further support for the DUC mechanism operating in the excitation range where IR-806 absorbs, and 'direct' upconversion by the nanoparticles operating in the range where the nanoparticles absorb.

In conclusion, we have demonstrated that dye-sensitized upconversion of nanoparticles yields a dramatically increased upconversion efficiency. Further improvement can be obtained by optimization of the dye emission and nanoparticle absorption spectral overlap. Moreover, we propose that by using suitable co-sensitizing sets of antenna molecules and upconverting nanoparticles, together absorbing the full desired spectral range of light to be upconverted, it will be possible to obtain even greater broadband upconversion. Such broadband sensitization, in combination with higher quantum yield upconverters, would change upconversion from an academic and exotic phenomenon into a realistic and viable tool for increasing the efficiency of photovoltaic devices. Furthermore, as the absorption spectrum of the dye-sensitized upconverter can be tuned, analyses and imaging techniques in medicine and diagnostics[13] based on upconverting nanoparticles will also benefit greatly from the proposed approach.

Methods

Synthesis of IR-806. The functionalization reaction was performed using standard Schlenk-line techniques in dry glassware and under a dry nitrogen atmosphere. A mixture of IR-780 iodide (2-[2-[2-chloro-3-[(1,3-dihydro-3,3-dimethyl-1-propyl-2*H*-indol-2-ylidene)ethylidene]-1-cyclohexen-1-yl]ethenyl]-3,3-dimethyl-1-propylindolium iodide; 500 mg, 0.75 mmol) and 4-mercaptobenzoic acid (231 mg, 1.50 mmol) in dimethylformamide (DMF) (20 ml) was stirred at room temperature for 17 h. DMF was removed under vacuum at 40 °C, and the residue was dissolved in CH_2Cl_2 (5 ml). The solution was filtered through a 0.45 μm polytetrafluoroethylene syringe filter and diethyl ether (150 ml) was added slowly to precipitate the product. The precipitate was collected by centrifugation, washed with diethyl ether, and dried under vacuum to afford 506 mg (0.65 mmol, 86%) of gold-coloured crystals. For characterization data see Supplementary Information.

Synthesis of $NaYF_4$:Yb,Er and $NaYF_4$ nanoparticles. $NaYF_4$:Yb,Er nanoparticles were synthesized according to a method described in the literature[29]. The reaction was performed using standard Schlenk-line techniques in dry glassware under a dry N_2 atmosphere. CF_3COONa (544 mg, 4 mmol), $Y(CF_3COO)_3{\cdot}3H_2O$ (752 mg, 1.56 mmol), $Yb(CF_3COO)_3{\cdot}3H_2O$ (226 mg, 0.40 mmol), $Er(CF_3COO)_3{\cdot}3H_2O$ (23 mg, 0.04 mmol) and oleylamine (20 ml) were added to a 100 ml three-neck round-bottom flask. With vigorous stirring, the mixture was heated to 100 °C at reduced pressure for 0.5 h to remove water and oxygen; heating was then continued up to 340 °C in the presence of nitrogen. After 1 h at 340 °C, heating was stopped. When the reaction temperature reached 80 °C, ethanol (150 ml) was added. The nanoparticles were isolated by centrifugation. The as-precipitated nanoparticles were washed three times with ethanol and then dispersed in 5 ml of chloroform. Undoped $NaYF_4$ nanoparticles were synthesized similarly, without the addition of the Yb and Er salts.

Sample preparation for UV-vis-NIR absorption and fluorescence measurements. All samples were prepared and measured under an atmosphere of nitrogen. The samples for UV-vis-NIR absorption and standard fluorescence measurements were prepared by adding different amounts of $NaYF_4$:Yb,Er nanoparticles to 0.01 mg of IR-806 in $CHCl_3$ (4 ml). The solutions were then stirred for 2 h at room temperature. The samples for upconversion fluorescence measurements were prepared by adding different amounts of IR-806 to 40 mg of $NaYF_4$:Yb,Er nanoparticles in $CHCl_3$ (1 ml). The solutions were stirred for 2 h at room temperature, then diluted 50 times for measurement.

Spectroscopy. For the upconversion luminescence measurements, a Ti:sapphire laser system (MIRA-900-F) was used as the excitation source. Luminescence spectra and lifetime measurements were performed in c.w. and pulsed modes (repetition rate of 76 MHz), respectively. The excitation light was focused into a 1-mm-thick sample cell by a lens with a focal length of 75 mm. This resulted in a focal spot of 35 ± 10 μm (FWHM) level. The excitation power was controlled by a gradient neutral density filter and set at 2 mW for all experiments, with the exception of the power-dependence measurements. The emission was collected with a right-angled geometry by an $f/2$ collimating lens and subsequently focused by an $f/4$ lens onto the slit of the spectrograph. The (time-resolved) emission detection was performed using a streak camera system equipped with a spectrograph (Hamamatsu C5680) running with the vertical time axis sweep off while recording c.w. emission spectra.

Received 17 April 2012; accepted 9 June 2012; published online 15 July 2012

References

1. Shockley, W. & Queisser, H. J. Detailed balance limit of efficiency of p–n junction solar cells. *J. Appl. Phys.* **32,** 510–519 (1961).
2. Conibeer, G. Third-generation photovoltaics. *Mater. Today* **10,** 42–50 (2007).
3. Wang, H.-Q., Batentschuk, M., Osvet, A., Pinna, L. & Brabec, C. J. Rare-earth ion doped up- conversion materials for photovoltaic applications. *Adv. Mater.* **23,** 2675–2680 (2011).
4. Van der Ende, B. M., Aarts, L. & Meijerink, A. Lanthanide ions as spectral converters for solar cells. *Phys. Chem. Chem. Phys.* **11,** 11081–11095 (2009).
5. De Wild, J., Meijerink, A., Rath, J. K., van Sark, W. G. J. H. M. & Schropp, R. E. I. Upconverter solar cells: materials and applications. *Energy Environ. Sci.* **4,** 4835–4848 (2011).
6. Strümpel, C. *et al.* Modifying the solar spectrum to enhance silicon solar cell efficiency—an overview of available materials. *Sol. Energy Mater. Sol. Cells* **91,** 238–249 (2007).
7. Trupke, T., Shalav, A., Richards, B. S., Würfel, P. & Green, M. A. Efficiency enhancement of solar cells by luminescent up-conversion of sunlight. *Sol. Energy Mater. Sol. Cells* **90,** 3327–3338 (2006).
8. Shalav, A., Richards, B. S., Trupke, T., Kramer, K. W. & Gudel, H. U. Application of $NaYF_4:Er^{3+}$ up-converting phosphors for enhanced near-infrared silicon solar cell response. *Appl. Phys. Lett.* **86,** 013505 (2005).
9. Shan, G.-B. & Demopoulos, G. P. Near-infrared sunlight harvesting in dye-sensitized solar cells via the insertion of an upconverter-TiO_2 nanocomposite layer. *Adv. Mater.* **22,** 4373–4377 (2010).
10. De Wild, J., Rath, J. K., Meijerink, A., van Sark, W. G. J. H. M. & Schropp, R. E. I. Enhanced near-infrared response of a-Si:H solar cells with β-$NaYF_4:Yb^{3+}$ (18%), Er^{3+} (2%) upconversion phosphors. *Sol. Energy Mater. Sol. Cells* **94,** 2395–2398 (2010).
11. Fischer, S. *et al.* Enhancement of silicon solar cell efficiency by upconversion: optical and electrical characterization. *J. Appl. Phys.* **108,** 044912 (2010).
12. Shalav, A., Richards, B. S. & Green, M. A. Luminescent layers for enhanced silicon solar cell performance: up-conversion. *Sol. Energy Mater. Sol. Cells* **91,** 829–842 (2007).
13. Haase, M. & Schäfer, H. Upconverting nanoparticles. *Angew. Chem. Int. Ed.* **50,** 5808–5829 (2011).
14. Baluschev, S. *et al.* Up-conversion fluorescence: noncoherent excitation by sunlight. *Phys. Rev. Lett.* **97,** 143903–06 (2006).

15. Baluschev, S. *et al.* A general approach for non-coherently excited annihilation up-conversion: transforming the solar-spectrum. *New J. Phys.* **10,** 013007 (2008).
16. Cheng, Y. Y. *et al.* Improving the light-harvesting of amorphous silicon solar cells with photochemical upconversion. *Energy Environ. Sci.* **5,** 6953–6959 (2012).
17. Boyer, J.-Ch. & van Veggel, F. C. J. M. Absolute quantum yield measurements of colloidal NaYF4: Er^{3+}, Yb^{3+} upconverting nanoparticles, *Nanoscale* **2,** 1417–1419 (2010).
18. Auzel, F. Upconversion and anti-Stokes processes with *f* and *d* ions in solids. *Chem. Rev.* **104,** 139–173 (2004).
19. Wang, F. & Liu, X. Recent advances in the chemistry of lanthanide-doped upconversion nanocrystals. *Chem. Soc. Rev.* **38,** 976–989 (2009).
20. Gamelin, D. R. & Güdel, H. U. Design of luminescent inorganic materials: new photophysical processes studied by optical spectroscopy. *Acc. Chem. Res.* **33,** 235–242 (2000).
21. Verhagen E., Kuipers, L. & Polman A. Enhanced nonlinear optical effects with a tapered plasmonic waveguide. *Nano Lett.* **7,** 334–337 (2007).
22. Rai, V. K. *et al.* Frequency upconversion in a Pr^{3+} doped chalcogenide glass containing silver nanoparticles. *J. Appl. Phys.* **103,** 093526 (2008).
23. Kassab, L. R. P. *et al.* Energy transfer and frequency upconversion in Yb^{3+}–Er^{3+}-doped PbO–GeO_2 glass containing silver nanoparticles. *Appl. Phys. B* **94,** 239–242 (2009).
24. Schietinger, S., Aichele, T., Wang, H., Nann, T. & Benson, O. Plasmon-enhanced upconversion in single $NaYF_4$:Yb^{3+}/Er^{3+} codoped nanocrystals. *Nano Lett.* **10,** 134–138 (2010).
25. Zhang, H. *et al.* Plasmonic modulation of the upconversion fluorescence in $NaYF_4$:Yb/Tm hexaplate nanocrystals using gold nanoparticles or nanoshells. *Angew. Chem. Int. Ed.* **49,** 2865–2868 (2010).
26. Sudheendra, L., Ortalan, V., Dey, S., Browning, N. D. & Kennedy, I. M. Plasmonic enhanced emissions from cubic $NaYF_4$:Yb:Er/Tm nanophosphors. *Chem. Mater.* **23,** 2987–2993 (2011).
27. Liu, N., Qin, W., Qin, G., Jiang, T. & Zhao, D. Highly plasmon-enhanced upconversion emissions from Au@β-$NaYF_4$:Yb,Tm hybrid nanostructures. *Chem. Commun.* **47,** 7671–7673 (2011)
28. Blankenship, R. E. *Molecular Mechanisms of Photosynthesis* (Blackwell Science, 2002).
29. Yi, G. S. & Chow, G. M. Synthesis of hexagonal-phase $NaYF_4$:Yb,Er and $NaYF_4$:Yb,Tm nanocrystals with efficient up-conversion fluorescence. *Adv. Funct. Mater.* **16,** 2324–2329 (2006).

Acknowledgements
J.C.H., W.Z. and C.V. acknowledge financial support from the Joint Solar Programme (JSP 1) of the Stichting voor Fundamenteel Onderzoek der Materie (FOM). The authors thank M.C.A. Stuart for TEM measurements of the nanoparticles and H.M.M. Hesp for assistance with laser spectroscopy. This is the first publication by the FOM Focus Group Groningen, participating in the Dutch Institute for Fundamental Energy Research (DIFFER).

Author contributions
W.Z., C.V. and J.A.M. were responsible for the experimental work. J.C.H. conceived the project. J.C.H. and M.S.P. supervised the research. All authors discussed the results. The manuscript was written by W.Z., M.S.P. and J.C.H.

Additional information
The authors declare no competing financial interests. Supplementary information accompanies this paper at www.nature.com/naturephotonics. Reprints and permission information is available online at http://www.nature.com/reprints. Correspondence and requests for materials should be addressed to J.C.H.

CORRIGENDUM

Towards high-speed imaging of infrared photons with bio-inspired nanoarchitectures

Andrew D. Pris, Yogen Utturkar, Cheryl Surman, William G. Morris, Alexey Vert, Sergiy Zalyubovskiy, Tao Deng, Helen T. Ghiradella & Radislav A. Potyrailo

Nature Photon. **6,** 195–200 (2012); published online 12 February 2012; corrected after print 11 July 2012.

In the version of this Article originally published, the measured temperature difference ΔT was at the detector plane, whereas the definition of noise-equivalent temperature difference (NETD) in equation (2) requires ΔT to be a thermal scene temperature difference. Thus, the NETD terminology in equation (2) has now been replaced with temperature sensitivity (TS). This error has been corrected in the HTML and PDF versions of the Article.

Appl Phys B
DOI 10.1007/s00340-008-3249-2

Applied Physics B
Lasers and Optics

Energy transfer and frequency upconversion in Yb^{3+}–Er^{3+}-doped $PbO\text{-}GeO_2$ glass containing silver nanoparticles

L.R.P. Kassab · F.A. Bomfim · J.R. Martinelli · N.U. Wetter · J.J. Neto · Cid B. de Araújo

Received: 29 July 2008

Abstract We report the infrared-to-visible frequency upconversion in Er^{3+}–Yb^{3+}-codoped $PbO\text{-}GeO_2$ glass containing silver nanoparticles (NPs). The optical excitation is made with a laser at 980 nm in resonance with the $^2F_{5/2} \rightarrow {}^2F_{7/2}$ transition of Yb^{3+} ions. Intense emission bands centered at 525, 550, and 662 nm were observed corresponding to Er^{3+} transitions. The simultaneous influence of the $Yb^{3+} \rightarrow Er^{3+}$ energy transfer and the contribution of the intensified local field effect due to the silver NPs give origin to the enhancement of the whole frequency upconversion spectra.

PACS 42.70.Ce · 78.55.-m · 78.55.Qr · 78.90.+t · 81.05.Pj

Phenomena related to the interaction of light with rare-earth-doped (RE-doped) glasses containing metallic nanoparticles (NPs) have been attracting large attention due to their relevance for a variety of applications such as colored displays, optical amplifiers as well as optical sensors. In particular, the surface-plasmon-enhanced (SP-enhanced) luminescence observed in RE-doped glasses containing metallic NPs has been studied by many authors [1–11].

Among the systems of interest the heavy metal oxide (HMO) glasses are known as excellent materials for photonic applications because of their specific characteristics such as: large mechanical resistance, high chemical durability and thermal stability, large transmission window (from 400 to 4500 nm), high refractive index, large nonlinear optical response, and low cutoff phonon energy (400–800 cm^{-1}) [1].

In the past years the synthesis and the characterization of HMO glasses doped with RE ions and containing metallic NPs were reported [7–11]. For instance, down-conversion luminescence enhancement was reported for Pr^{3+}-doped lead-germanate oxide (PGO) glass containing silver NPs [7]. The increase of Eu^{3+} luminescence due to the presence of gold NPs in tellurite glasses was observed and characterized [8]. Studies of SP-enhanced frequency upconversion (UC) in Pr^{3+}-doped tellurium-oxide glasses with silver NPs were reported in [9].

Also, recently we have demonstrated enhancement of ∼100% in the infrared-to-green UC process in Er^{3+}-doped PGO glass containing silver NPs [10]. The excitation was made at 980 nm and the growth of the UC intensity at 530 and 550 nm was attributed to the increased local field in the proximity of the NPs. Unfortunately, even in the presence of the NPs the UC luminescence of the Er^{3+}-doped PGO is limited by the relatively small absorption cross-section of Er^{3+} ions at 980 nm. The red luminescence at 662 nm having wavelength far from the SP resonance wavelength, λ_{SP}, is less influenced by the presence of spherical silver NPs. However, it may be intensified if particles with different shapes and aggregates of NPs are present. On the other hand, PGO glass doped with Er^{3+} and Yb^{3+}, without silver

L.R.P. Kassab
Laboratório de Vidros e Datações da FATEC-SP, CEETEPS/UNESP, 01124-060 São Paulo, SP, Brazil

F.A. Bomfim · J.R. Martinelli
Centro de Ciências e Tecnologia de Materiais—IPEN, 05508-900 São Paulo, SP, Brazil

N.U. Wetter · J.J. Neto
Centro de Lasers e Aplicações—IPEN, 05508-900 São Paulo, SP, Brazil

C.B. de Araújo (✉)
Departamento de Física, Universidade Federal de Pernambuco, 50670-901 Recife, PE, Brazil
e-mail: cid@df.ufpe.br

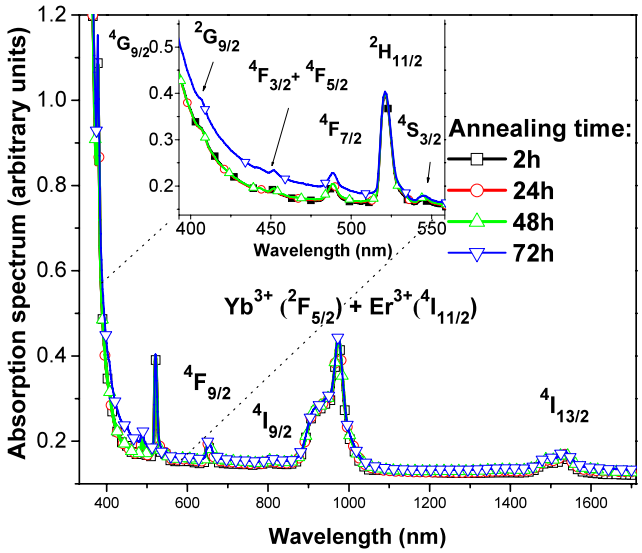

Fig. 1 Absorption spectra of Er^{3+}–Yb^{3+}-codoped PbO-GeO_2 glasses containing silver NPs for different heat-treatment durations

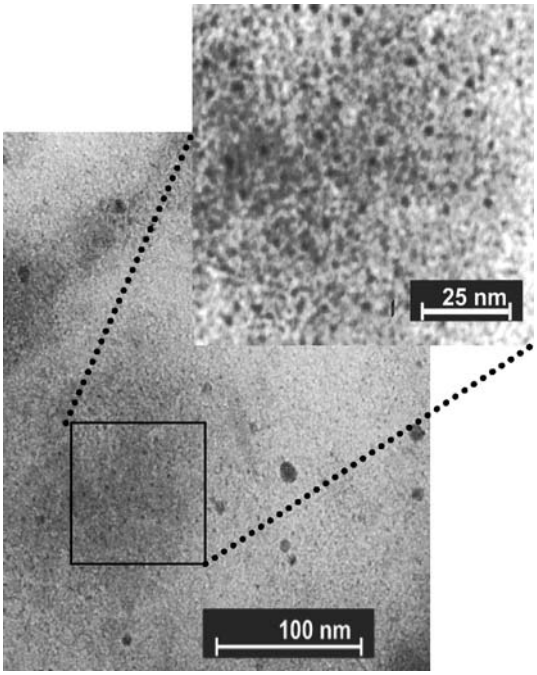

Fig. 2 TEM images of the samples annealed for 48 h at 420°C

NPs, present increased red luminescence due to the energy transfer (ET) from Yb^{3+} to Er^{3+} ions [12, 13].

In this letter we demonstrate improvement of the UC luminescence efficiency of Er^{3+} ions in PGO glass containing silver NPs by codoping the samples with Yb^{3+} ions. We show that the combined effect of the silver NPs and the efficient ET from resonantly excited Yb^{3+} ions contribute to the enhancement of the whole UC spectrum. The large absorption cross-section of the Yb^{3+} ions at 980 nm allows the increase of the red luminescence in such a way that it may reach intensities comparable with the green emissions.

The PGO glass composition studied was 41 PbO-59 GeO_2 (in mol%). For the experiments we added 0.5 wt% of Er_2O_3, 3.0 wt% of Yb_2O_3, and 1.0 wt% of $AgNO_3$ to the original composition. The samples were obtained by melting the starting oxide powders in an alumina crucible for 1 h at 1200°C, quenching and annealing in air in a preheated brass mold, and annealing at 420°C for 2 h. After the cooling the samples were polished and then annealed for different durations ($\tau_A = 24$, 48, and 72 h) to reduce the Ag^+ ions to Ag^0, in order to nucleate silver NPs.

Transmission electron microscopy (TEM) using a 200 kV equipment was performed to investigate the nucleation and growth of the NPs.

The linear optical absorption spectra were measured at room temperature in the 300–1700 nm range and the frequency UC spectra (infrared-to-visible conversion) were excited with a CW diode laser (7 W, 980 nm). The luminescence signal was dispersed by a monochromator fitted with a photomultiplier.

Figure 1 presents the absorption spectra of the Er^{3+}–Yb^{3+}-codoped PGO glass containing silver NPs in the visible and in the near-infrared regions. Absorption bands attributed to the $4f$–$4f$ transitions of Er^{3+} ions corresponding to the transitions starting from the ground state ($^4I_{15/2}$) to the excited states are observed. The intense absorption band at ≈980 nm is mainly due to the $^2F_{7/2} \rightarrow {}^2F_{5/2}$ transition of Yb^{3+} ions that overlaps with the weaker $^4I_{15/2} \rightarrow {}^4I_{11/2}$ transition of the Er^{3+} ions. The absorption band related to the SP is not observed because the amount of the NPs is not enough to originate a strong band. With the basis on the dielectric function of silver [14] and the refractive index of PGO glass (≈2), we estimated λ_{SP} to be located in the range of ∼420 to ∼500 nm. However, the presence of the silver NPs in the PGO samples is confirmed by electron microscopy.

Figure 2 shows a TEM image corresponding to the sample annealed for 48 h at 420°C. The metallic NPs have average diameter of 2.5 nm but we also observed the presence of larger particles and aggregates. The samples heat-treated for shorter time intervals present NPs with smaller average diameter.

Figure 3a shows the emission spectra of the Er^{3+}–Yb^{3+}-codoped PGO samples for different anneal durations, τ_A. Emission bands centered at 525, 550, and 662 nm that correspond to the transitions $^2H_{11/2} \rightarrow {}^4I_{15/2}$, $^4S_{3/2} \rightarrow {}^4I_{15/2}$, and $^4F_{9/2} \rightarrow {}^4I_{15/2}$, respectively, are observed. Figure 3b shows that the relative intensity of the UC bands can be adjusted by an appropriate choice of τ_A that controls the amount of silver NPs formed in the sample.

Figure 4 presents a simplified energy level diagram for the Er^{3+} and the Yb^{3+} ions. Because the laser wavelength is in resonance with the transition $^2F_{5/2} \rightarrow {}^2F_{7/2}$ (Yb^{3+}) and

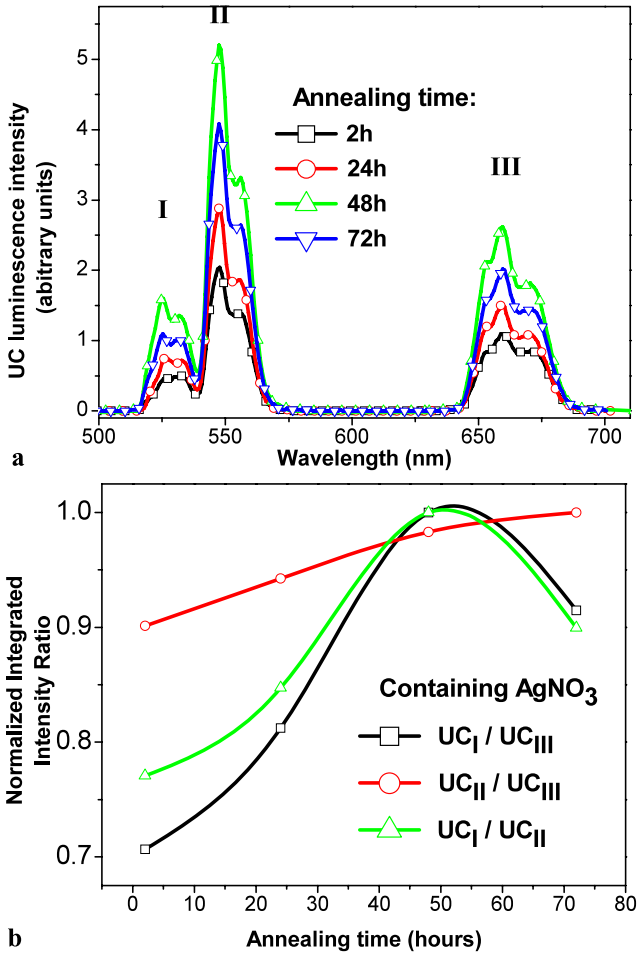

Fig. 3 (**a**) Frequency UC spectra for excitation at 980 nm. (**b**) Normalized integrated UC intensity as a function of the annealing time

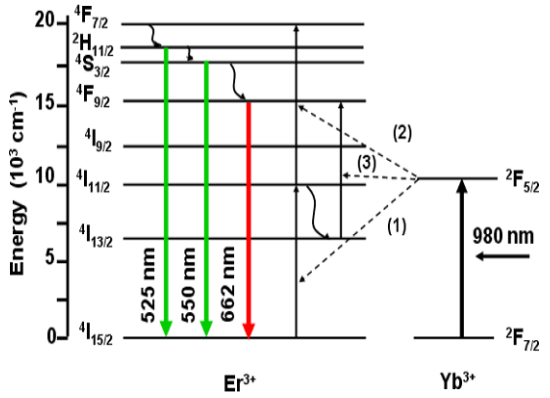

Fig. 4 Energy level diagram of Er^{3+} and Yb^{3+} ions illustrating possible UC pathways for the Er^{3+}–Yb^{3+}-codoped glasses. The *solid straight lines* with upward and downward arrows indicate optical transitions; *dotted lines* and *wavy arrows* denote ET processes and nonradiative relaxation, respectively

because its oscillator strength is much greater than the one corresponding to the transition $^4I_{15/2} \rightarrow {}^4I_{11/2}$ (Er^{3+}), we attribute the excitation of levels $^4S_{3/2}$ and $^4F_{9/2}$ in Er^{3+} ions mainly to the ET from Yb^{3+} ions. The ET efficiency depends on the relative concentration of Er^{3+} and Yb^{3+} and the lifetime of the levels participating in the ET process.

There are two possible efficient ET pathways [12, 13] as indicated in Fig. 4 by the dashed lines 1, 2, and 3. The green emissions are mainly originated by the following process: Yb^{3+} ions are excited from the ground state to the $^2F_{5/2}$ multiplet under 980 nm pumping; the excited ions transfer the stored energy to the Er^{3+} ions that are promoted from the ground state to the $^4I_{11/2}$ state. Then, a second ET event promotes the Er^{3+} ions from the $^4I_{11/2}$ level to the $^4F_{7/2}$ level (steps (1) and (2)—dashed lines in the Fig. 4). Following this transition, the Er^{3+} ion relaxes nonradiatively to the $^2H_{11/2}$ and $^4S_{3/2}$ levels. Afterwards, the $^2H_{11/2} \rightarrow {}^4I_{15/2}$ and $^4S_{3/2} \rightarrow {}^4I_{15/2}$ transitions originate the green emissions. The proximity between the green luminescence wavelengths and λ_{SP} favors the intensity enhancement that is due to the increased local field resulting from the mismatch between the dielectric functions of the silver NPs and the glass.

The red emission at 662 nm is due to the $^4F_{9/2} \rightarrow {}^4I_{15/2}$ transition. Besides the feeding of the $^4F_{9/2}$ level through the nonradiative relaxation from the $^4S_{3/2}$ level, the ET event represented by 3 in Fig. 4 may occur following the nonradiative transition $^4I_{11/2} \rightarrow {}^4I_{13/2}$. The longer lifetime of the $^4I_{13/2}$ level compared with the lifetime of the $^4I_{11/2}$ level [1] makes channel 3 dominant over channels 1 and 2; consequently, the red emission is enhanced. Moreover, as shown in Fig. 3, the red emission is also intensified for larger values of τ_A. This is attributed to the nucleation of larger silver NPs and aggregates as observed for Pr^{3+} in [7, 9]. Notice that the red intensity illustrated in Fig. 3 becomes comparable with the intensity of transitions $^2H_{11/2} \rightarrow {}^4I_{15/2}$ and $^4S_{3/2} \rightarrow {}^4I_{15/2}$ for $\tau_A \approx 40$ h. We also note from Fig. 3b that the ratio UC_I/UC_{II} between the integrated intensities of transitions centered at 525 and 550 nm changes from 0.77 (for $\tau_A \approx 0$) to ~1.0 (for $\tau_A \approx 50$ h). This behavior is understood considering that the transition at 525 nm is closest to λ_{SP} than 550 nm.

In summary, with the present results we demonstrated the simultaneous exploitation of the enhanced local field contribution due to silver NPs and energy transfer processes between two different rare-earth (RE) ions in order to control the luminescence spectrum of a glassy composite material. This approach can be applied for different RE ions in order to improve the efficiency of luminescent glasses.

Acknowledgements Financial support of the Brazilian Agencies (CNPq and FACEPE) is acknowledged. The Laboratório de Microscopia Eletrônica (IFUSP) is also acknowledged for the TEM images. This work was performed under the Nanophotonics Network Project.

References

1. M. Yamane, Y. Asahara, *Glasses for Photonics* (Cambridge University Press, Cambridge, 2000)
2. P.N. Prasad, *Nanophotonics* (Wiley, New York, 2004)
3. O.L. Malta, P.A.S. Cruz, G.F. de Sá, F. Auzel, J. Lumin. **33**, 261 (1985)
4. T. Hayakawa, S.T. Selvan, M. Nogami, Appl. Phys. Lett. **74**, 1513 (1999)
5. C. Strohhöfer, A. Polman, Appl. Phys. Lett. **81**, 1414 (2002)
6. J. Kalkman, L. Kuipers, A. Polman, Appl. Phys. Lett. **86**, 041113 (2005)
7. L.P. Naranjo, C.B. de Araújo, O.L. Malta, P.A.S. Cruz, L.R.P. Kassab, Appl. Phys. Lett. **87**, 241914 (2005)
8. R. de Almeida, D.M. da Silva, L.R.P. Kassab, C.B. de Araújo, Opt. Commun. **281**, 108 (2008)
9. V.K. Raí, L. de S. Menezes, C.B. de Araújo, L.R.P. Kassab, D.M. da Silva, R.A. Kobayashi, J. Appl. Phys. **103**, 093526 (2008)
10. D.M. da Silva, L.R.P. Kassab, S.R. Luthi, C.B. de Araújo, A.S.L. Gomes, M.J.V. Bell, Appl. Phys. Lett. **90**, 081913 (2007)
11. L.R.P. Kassab, C.B. de Araújo, R.A. Kobayashi, R. de A. Pinto, D.M. da Silva, J. Appl. Phys. **102**, 103515 (2007)
12. F.A. Bomfim, J.R. Martinelli, L.R.P. Kassab, N.U. Wetter, J.J. Neto, J. Non-Cryst. Solids (2008, to be published)
13. L. Feng, J. Wang, Q. Tang, H. Hu, H. Liang, Q. Su, J. Non-Cryst. Solids **352**, 2090 (2006)
14. E.D. Palik, *Handbook of Optical Constants of Solids* (Academic Press, New York, 1985)